Available online at www.sciencedirect.com
ScienceDirect
Trans. Nonferrous Met. Soc. China 29(2019) 157−164
Transactions of Nonferrous Metals Society of China
www.tnmsc.cn

Microstructure and photocatalytic activity of Ni-doped ZnS nanorods prepared by hydrothermal method

Wen-hua ZHAO[1,2], Zhi-qiang WEI [1,2], Xiao-juan WU[1], Xu-dong ZHANG[2], Li ZHANG[2], Xuan WANG[1]

1. State Key Laboratory of Advanced Processing and Recycling Nonferrous Metals, Lanzhou University of Technology, Lanzhou 730050, China;
2. School of Science, Lanzhou University of Technology, Lanzhou 730050, China

Received 31 December 2017; accepted 28 May 2018

Abstract: Pure ZnS and Ni^{2+}-doped ZnS nanorods ($Zn_{1-x}Ni_xS$, x=0, 0.01, 0.03, 0.05 and 0.07, mole fraction, %) were synthesized by hydrothermal method. The effects of Ni^{2+} doping on the phase-structure, morphology, elemental composition and optical properties of the samples were investigated by X-ray diffraction (XRD), high-resolution transmission electron microscopy (HRTEM), X-ray energy dispersive spectrometry (EDS) and ultraviolet–visible spectroscopy (UV−Vis), respectively. The photocatalytic activity of $Zn_{1-x}Ni_xS$ nanorods was evaluated by the photodegradation of organic dyes Rhodamine B (RhB) in aqueous solution under UV light irradiation. The results show that all samples exhibit wurtzite structure with good crystallization. The morphologies are one-dimensional nanorods with good dispersion, and the distortion of the lattice constant occurs. The band gap of $Zn_{1-x}Ni_xS$ samples is smaller than that of pure ZnS, thus red shift occurs. Ni^{2+}-doped ZnS nanocrystals can enhance photocatalytic activities for the photodegradation of RhB. Especially, $Zn_{0.97}Ni_{0.03}S$ sample exhibits better photocatalytic performance and photocatalytic stability for the decomposition of RhB.

Key words: $Zn_{1-x}Ni_xS$ nanorods; phase-structure; microstructure; photocatalytic activity; hydrothermal method

1 Introduction

With the industry development, population growth and urbanization, the increasing pollution of natural water and air has become one of the considerable challenges to the modern human society and eco-system [1−3]. The main contamination source is artificial dyes which are non-biodegradable and toxic. The poisonous complexes in water media create awful hazard to the human health. Various treatment techniques have been applied for eradicating the dangerous pigments from wastewater, including coagulation−flocculation, centrifugation, ion exchange, sedimentation, membrane filtration, adsorption, photocatalysis and distillation. Compared with the traditional techniques, nanocrystalline semiconductor photocatalysis is a promising and effective technique for photocatalytic degradation of the pollutants and toxins due to their advantages such as nontoxic, inexpensive, strong oxidizing activity and chemical stability [4].

ZnS is a multifunctional n-type semiconductor material with a wide direct band gap of 3.67 eV and a free exciting binding energy of 60 MeV [5,6]. ZnS semiconductor nanocrystals exhibit novel properties and wide application prospect such as solid state solar-cells, optoelectronic devices, energy storage, biosensors, ultraviolet detectors, gas-sensing devices and photocatalysis [7,8]. In recent years, some researchers have studied transition metal ions doped ZnS semiconductor nanocrystals to explore photoluminescence properties and room-temperature ferromagnetism by providing extra positive carriers in the host material [9−11]. The crystal structure and band structure of ZnS nanocrystals can be modified by controlling the preparation process, changing the kinds and amount of doping elements, further improving the magnetic and optical properties [12,13]. Furthermore, doping with transition metal ion configurations could significantly improve the separation rate of photo-induced charge carriers in semiconductor photocatalysts, which inhibits the recombination of photogenerated electron−hole pairs

Foundation item: Project (51261015) supported by the National Natural Science Foundation of China; Project (1308RJZA238) supported by the Natural Science Foundation of Gansu Province, China
Corresponding author: Zhi-qiang WEI; Tel: +86-931-2973780; E-mail: qianweizuo@163.com
DOI: 10.1016/S1003-6326(18)64924-6

and enhances the photocatalytic activity greatly.

However, to the best of our knowledge, there are rare reports about the effect of doping concentration on the photocatalytic properties of transition metal ions doped ZnS nanocrystals. Therefore, the main aim of this study is to investigate the influences of Ni^{2+} doping on the microstructure and photocatalytic activity of transition metal ions doped ZnS nanocrystals at different doping contents. In this study, $Zn_{1-x}Ni_xS$ nanocrystals with different doping contents (x=0, 0.01, 0.03, 0.05 and 0.07, mole fraction, %) were synthesized by hydrothermal method. The effects of Ni^{2+} doping content on the phase-structure, morphology, elemental composition, optical properties and photocatalytic activity of the as-prepared samples were studied and compared. Moreover, the possible photocatalytic mechanism was discussed.

2 Experimental

2.1 Synthesis mechanism

$Zn_{1-x}Ni_xS$ (x=0, 0.01, 0.03, 0.05 and 0.07) nanocrystals were prepared by hydrothermal method [14]. All raw materials used were analytical grade without further purification. The manufacturing process was as follows: according to the chemical formula $Zn_{1-x}Ni_xS$ and the mole ratio of the metal cation, weighed stoichiometric $Zn(Ac)_2{\cdot}2H_2O$, $(NH_2)_2CS$ and $NiCl_2{\cdot}6H_2O$ were dissolved in 80 mL ethylenediamine ($C_2H_8N_2$) and deionized water (1:1 in volume ratio) to obtain a solution. The mixture was magnetically stirred at room temperature until the solution mixed uniformly for 1 h. Then, the resulting mixed solution was transferred into a 100 mL Teflon-lined stainless steel autoclave. The hydrothermal reaction process was conducted at 200 °C for 12 h in an oven. At the end of the reaction, the autoclave was cooled to room temperature naturally. The resulting precipitate was separated centrifugally and washed with distilled water and absolute alcohol several times, respectively. The obtained products were dried in an oven at 60 °C for 10 h. Thus, $Zn_{1-x}Ni_xS$ nanocrystals were collected and used for further studies.

2.2 Characterization techniques

The crystal structure and phase of as synthesized samples were determined by a powder X-ray diffractometer (Japan Rigaku D/Max−2400) with Cu K_α radiation at λ=1.54056 Å. The samples were scanned in a 2θ range from 10° to 90° with a scanning rate of 0.005 (°)/s and a step size of 0.02°. The average crystalline grain size of the products was estimated from the half maximum width and the peak position of an XRD line broadened according to the Scherer formula. The morphology and microstructure of the samples were observed by high-resolution transmission electron microscopy (HRTEM, JEM−2010). The mole fraction of the products was verified by X-ray energy dispersive spectroscopy (EDS). The absorption spectra were analyzed using ultraviolet–visible (UV−Vis, TU−1901) spectrophotometer.

2.3 Measurement of photocatalytic activity

The photocatalytic activities of pure ZnS and Ni^{2+}-doped ZnS nanorods were investigated by monitoring the decolorization of Rhodamine B (RhB) in an aqueous solution under UV light irradiation at room temperature. In a typical process, 50 mg of photocatalyst powder was added to 100 mL RhB aqueous solution with an initial concentration of 10 mg/L. The mixed suspension was magnetically stirred in a quartz beaker in the dark for 30 min to ensure the adsorption−desorption equilibrium of the prepared catalysts and organic dye molecules in the reaction system. Then, the colloidal solution was irradiated by using a UV light mercury lamp with the central wave length of 365 nm as the light source. The photocatalytic experiment was conducted at room temperature in a cylindrical glass vessel, and the colloid surface was maintained a distance of 30 cm from the light source to avoid heat effect. During the photocatalytic process, approximately 3 mL irradiated suspension was sampled periodically. The UV−Vis spectrum of the supernatant after centrifugation was recorded to observe the adsorption and degradation performance. For the assessment of organic pollutant degradation, typical absorption peak of RhB at 554 nm was chosen as a reference point in absorption spectra. The photocatalytic degradation rate (η) is defined as the following equation: $\eta=(C_0-C_t)/C_0\times100\%$, where C_0 is the initial concentration of RhB and C_t means the concentration of RhB after light irradiation for time t.

3 Results and discussion

3.1 Phase composition

The XRD patterns of $Zn_{1-x}Ni_xS$ (x=0, 0.01, 0.03, 0.05 and 0.07) nanomaterials are shown in Fig. 1. The diffraction peaks are well ascribed to the reflection of (100), (002), (101), (102), (110), (103) and (112) crystallographic planes of ZnS, respectively. The samples possess single-phase ZnS wurtzite structure (JCPDS card No. 36−1450) with lattice parameters a=3.829 Å and c=6.279 Å. No extra peaks of the secondary phases such as metal clusters or metal oxides are observed when the mole fraction of Ni^{2+} ranges from 1% to 5% in the XRD patterns, which indicates that all Ni^{2+} effectively substitute Zn^{2+} sites in the ZnS host lattice without

changing the wurtzite structure of the parent ZnS. However, the NiS peaks appearing in the sample $Zn_{0.93}Ni_{0.07}S$ reveal that doping 7% Ni is excessive.

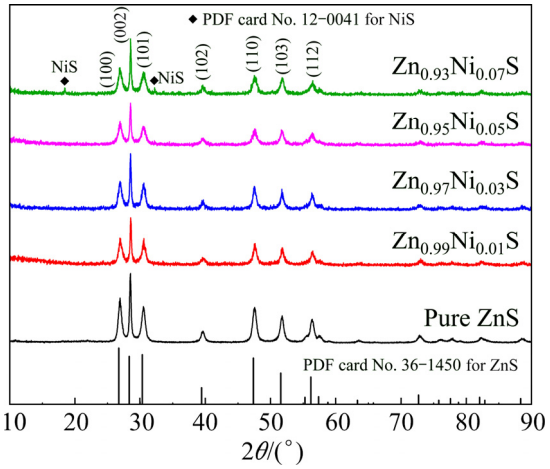

Fig. 1 XRD patterns of $Zn_{1-x}Ni_xS$ (x=0, 0.01, 0.03, 0.05 and 0.07) nanorods

The average crystalline grain size of the products is estimated according to Scherrer formula as follows:

$$D=\frac{K\lambda}{B\cos\theta} \quad (1)$$

where D represents the average crystalline size, K(=0.89) is the Scherrer constant, λ is the X-ray wavelength (Cu K_α, λ=1.54056 Å), θ is the Bragg angle and B represents the full width at half maximum of the (002) plane. The crystallite size of the samples is summarized in Table 1. It has been observed that the diffraction peak of the (002) plane gradually increases with increase of Ni^{2+} content and the crystallite size decreases from 35 to 29 nm with increase of Ni^{2+} content from 0 to 7%. The lattice constants a and c are calculated by the crystallographic formula:

$$a=d_{hkl}\sqrt{\frac{4}{3}(h^2+hk+l^2)+\left(\frac{a}{c}\right)^2 l^2} \quad (2)$$

The corresponding parameters of the diffraction peak (002) for undoped and doped ZnS samples are shown in Table 1. The lattice constant and inter planar distance of Ni^{2+}-doped ZnS samples decrease as the doped Ni^{2+} content increases. This indicates that the changes in peak position, peak width and peak intensity depend on the lattice parameter because the Ni^{2+} occupies Zn^{2+} sites in the wurtzite matrix.

3.2 Morphology

HRTEM is a versatile technique to estimate particle size distribution and structural information. The morphologies of the pure ZnS nanocrystals are high quality one-dimensional nanorod structures in Figs. 2(a) and (b). The diameter is in the range of 10−20 nm, and the average is approximately 15 nm. Meanwhile, the average length is about 100 nm. Compared with pure ZnS, the diameter and length of $Zn_{0.97}Ni_{0.03}S$ nanorods slightly become shorter and wider in Figs. 2(c) and (d). The diameter of $Zn_{0.97}Ni_{0.03}S$ sample is about 20 nm, and the length ranges from 100 to 200 nm, which reveals that a well oriented growth along the (002) direction possesses good crystallization with clear lattice fringe and no obvious defects. The fringe spacing is about 0.312 nm, which is close to the (002) inter planar distance of wurtzite ZnS structure. The shrink of crystal lattice occurs because the radius of Ni^{2+} (0.69 Å) is smaller than that of Zn^{2+} (0.74 Å).

Table 1 Parameters of XRD patterns for $Zn_{1-x}Ni_xS$ (x=0, 0.01, 0.03, 0.05 and 0.07) nanorods

Sample	2θ/(°)	d_{hkl}/Å	Lattice constant/Å		D/nm
			a	c	
Pure ZnS	28.40	3.139	3.829	6.279	35
$Zn_{0.99}Ni_{0.01}S$	28.49	3.130	3.824	6.261	33
$Zn_{0.97}Ni_{0.03}S$	28.52	3.128	3.815	6.255	31
$Zn_{0.95}Ni_{0.05}S$	28.62	3.117	3.805	6.234	30
$Zn_{0.93}Ni_{0.07}S$	28.84	3.093	3.777	6.190	29

The corresponding selected area electron diffraction (SAED) patterns of pure ZnS and $Zn_{0.97}Ni_{0.03}S$ samples consist of one center and many diffraction rings with different radii in insets of Figs. 2(b) and (d), respectively. The diffraction rings from inside to outside are corresponding to (100), (002), (101), (102), (110), (103) and (112) planes of wurtzite ZnS structure, which is in good agreement with the results of XRD patterns. This further indicates that all Ni^{2+} successfully substitutes the Zn^{2+} lattice site.

3.3 Chemical components

Figure 3 depicts the EDS spectra of the pure ZnS and $Zn_{0.97}Ni_{0.03}S$ nanorods to determine the composition of the samples. The spectra reveal that only the expected characteristic peaks of Zn and S elements are present in pure ZnS in Fig. 3(a). For $Zn_{0.97}Ni_{0.03}S$ nanorods, it also obviously confirms the presence of Ni element besides Zn and S elements. Within the detection limit of the instrument, no other impurity atoms are found in Fig. 3(b). The quantitative mole and mass fractions of the compositional elements are indicated in the inset of Fig. 3. The estimated mole fractions of Zn, Ni and S are very close to the nominal values. EDS results indicate that Ni^{2+}-doped ZnS samples are successful synthesized by hydrothermal method, further verifying XRD conclusion. Ni^{2+} ions are successfully substituted as dopant in $Zn_{0.97}Ni_{0.03}S$ matrix.

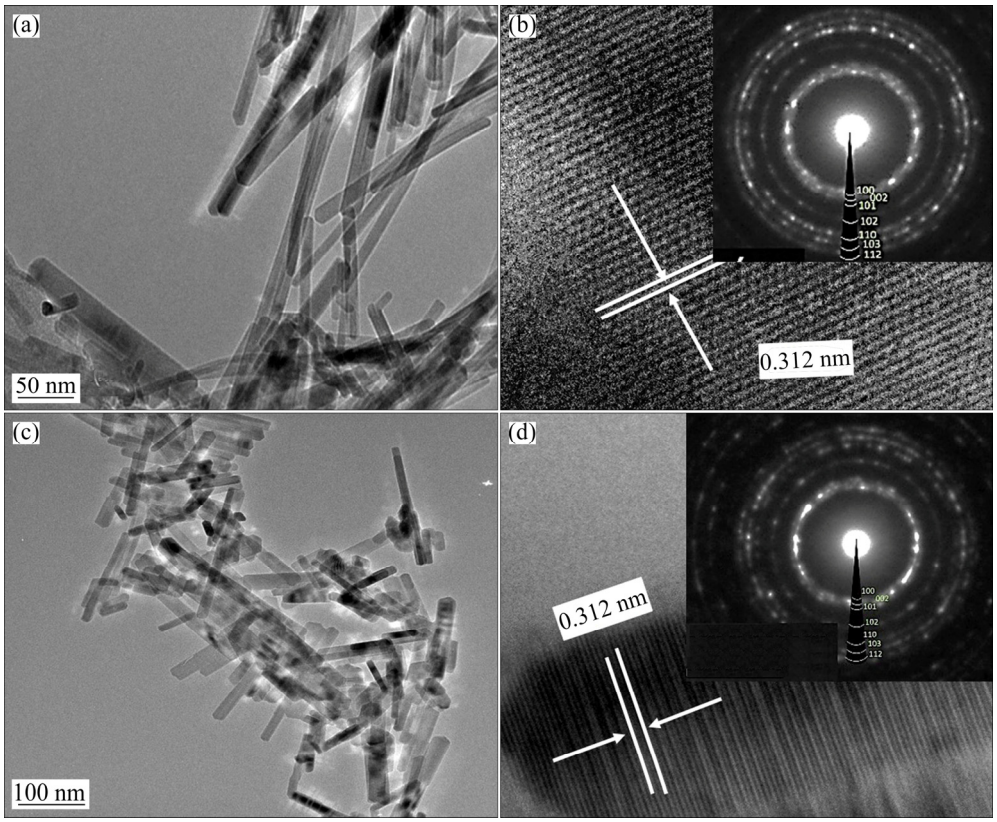

Fig. 2 HRTEM images (a, c) and SAED patterns (b, d) of pure ZnS (a, b) and $Zn_{0.97}Ni_{0.03}S$ (c, d) nanorods

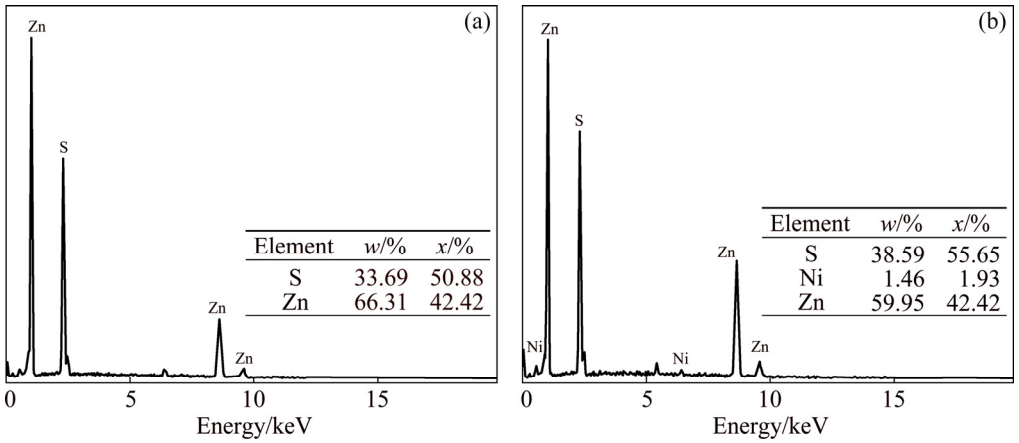

Fig. 3 EDS spectra of pure ZnS (a) and $Zn_{0.97}Ni_{0.03}S$ (b) nanorods

3.4 UV−Vis spectra

The UV−Vis absorption spectra for $Zn_{1-x}Ni_xS$ (x=0, 0.01, 0.03, 0.05 and 0.07) samples are recorded in Fig. 4. Ni^{2+}-doped ZnS samples exhibit an obvious enhanced absorbance in the UV light region (<350 nm) compared with pure ZnS. The optical band gap is calculated according to Tauc relation as follows [15]:

$$(\alpha hv)^{1/n} = A(hv - E_g) \quad (3)$$

where hv is the incident photon energy, v is the photic frequency, E_g is the optical band gap, A(=4πk/λ) represents the absorption coefficient, h is the Plank constant, k and λ represent the absorbance and wavelength, respectively, and α is the absorption coefficient, which is obtained using the Kubelka–Munk function:

$$\alpha=F(R)=(1-R)^2/(2R) \quad (4)$$

where R is the percentage of reflected light. For direct band gap ZnS nanocrystals, n=1/2, $(\alpha hv)^2$ gives the best linear fitting curve in the band edge region. The relationship between $(\alpha hv)^2$ and hv is represented by the inset of Fig. 4. The values of E_g are obtained by

extrapolating the linear region of the curve on $h\nu$ axis at $(\alpha h\nu)^2=0$. The estimated optical band gaps of $Zn_{1-x}Ni_xS$ (x=0, 0.01, 0.03, 0.05 and 0.07) samples are 3.79, 3.77, 3.74, 3.75 and 3.76 eV, respectively. It is obviously seen that the band gap of pure ZnS is higher than that of the doped ZnS, therefore red shift occurs. Furthermore, the band gaps of the doped ZnS decrease as Ni^{2+} doping content increases. It is critical that $Zn_{0.97}Ni_{0.03}S$ sample exhibits the minimum band gap (3.74 eV). The s−d and p−d interactions create positive corrections to the valance band and conduction band edges, respectively, leading to the band gap narrowing.

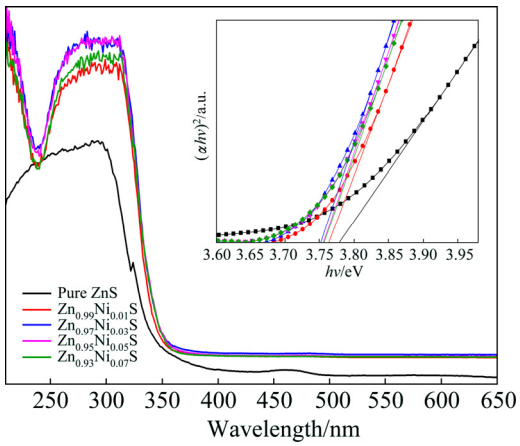

Fig. 4 UV−Vis absorption spectra of $Zn_{1-x}Ni_xS$ (x=0, 0.01, 0.03, 0.05 and 0.07) nanorods

3.5 Photocatalytic activity

In order to study the influence of doping content on the degradation rate, the photocatalytic activities of Ni^{2+}-doped ZnS nanorods were evaluated for the photodegradation of RhB in aqueous solution under UV light irradiation. Figure 5 shows the RhB degradation of $Zn_{1-x}Ni_xS$ samples with different doping contents versus time (t) under UV light irradiation. The RhB cannot be disintegrated in aqueous solution under UV light irradiation for 180 min, which reveals good stability without catalyst, implying good photocatalytic activity of $Zn_{1-x}Ni_xS$ (as catalyst) samples.

The degradation rate of pure ZnS for RhB after UV light irradiation for 180 min is 36.5%, exhibiting relatively high photocatalytic performance. Ni^{2+}-doped ZnS samples display greatly higher photocatalytic activities pure ZnS. The degradation rates for $Zn_{1-x}Ni_xS$ (x=0.01, 0.03, 0.05 and 0.07) are 94.04%, 98.53%, 91.21% and 86.82%, respectively. This demonstrates that the dopant in localized electronic states is served as photo-generated charge carrier traps under UV light irradiation. Furthermore, the photocatalytic activity of the doped ZnS increases with increasing the Ni^{2+} doping content from 0 to 3%, and it then decreases with further increasing Ni^{2+} doping content.

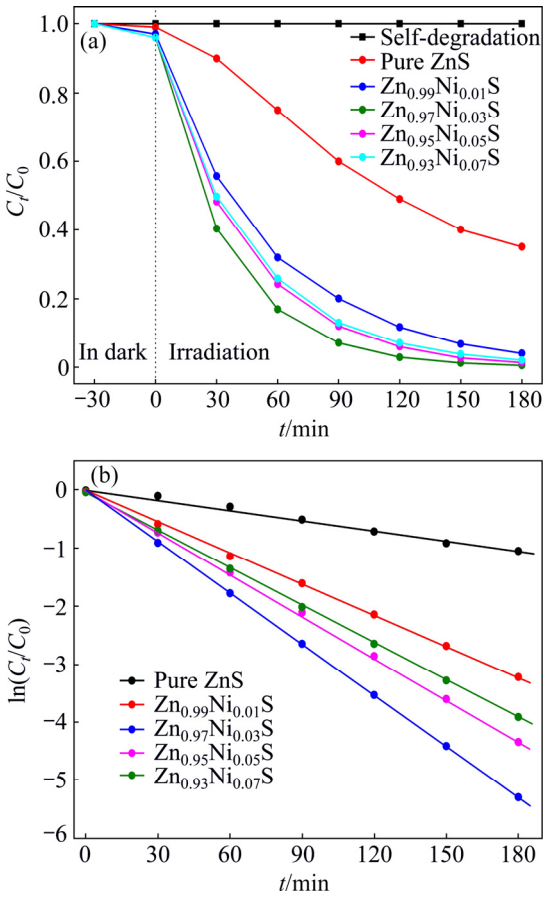

Fig. 5 Photocatalytic activities (a) and first-order kinetics plot (b) of $Zn_{1-x}Ni_xS$ (x=0, 0.01, 0.03, 0.05 and 0.07) nanorods

$Zn_{0.97}Ni_{0.03}S$ photocatalyst demonstrates the maximum degradation rate of 98.53%, which indicates that there exists an optimal doping content of 3% for catalysts to photodegrade RhB dyes. The increased photocatalytic activity of Ni^{2+}-doped ZnS nanorods is ascribed to the crystal structure and band structure of the semiconductor adjusted by doping Ni^{2+} ions. The doped Ni^{2+} ions are help to enhance the separation efficiency of electron−hole pairs. In addition, they effectively increase the transport of photogenerated carriers and recombination of electrons and holes, which is beneficial to the photocatalytic activities of RhB. However, excessive Ni^{2+} ions have a negative effect on the photocatalytic activity when the Ni^{2+} doping content exceeds 3% owing to the increase of recombination probability of electron−hole pairs.

The first-order kinetics plot of $Zn_{1-x}Ni_xS$ nanorods for the photodegradation of RhB is shown in Fig. 5(b). The degradation rate of the RhB accords well with pseudo-first-order kinetic equation:

$$\ln(C_t/C_0)=-kt \quad (5)$$

where C_t and C_0 are the concentrations at time t and

initial concentration of RhB, respectively, t is the irradiation time, and k denotes the apparent first-order reaction rate constant. The rate constant k is determined from the plot of $\ln(C_t/C_0)$ versus t. The k values of photocatalytic degradation rate for $Zn_{1-x}Ni_xS$ (x=0, 0.01, 0.03, 0.05 and 0.07) are 0.0058, 0.0177, 0.0292, 0.0239 and 0.0215 min^{-1}, respectively. The photocatalytic activities of Ni^{2+}-doped ZnS samples increase with increasing the Ni^{2+} doping content until reaching the maximum value firstly, and then decline with further increase of Ni^{2+} concentration. It is worthy to mention that the rate constant of the $Zn_{0.97}Ni_{0.03}S$ nanorods is 0.0292 min^{-1}, which is about four times larger than that of pure ZnS. Meanwhile, it is much higher than those of $Zn_{1-x}Ni_xS$ (x=0, 0.01, 0.05 and 0.07). Ni-doped ZnS samples could improve the photocatalytic performance under UV light irradiation, which is attributed to doped Ni^{2+} ions, predominantly narrowing the optical band gap and enhancing optical absorption intensity via recombination of electrons and holes.

The recycling reactions were carried out for the RhB photodegradation of $Zn_{0.97}Ni_{0.03}S$ sample to study the stability and reusability, as shown in Fig. 6(a). Even though the RhB photodegradation rate slightly decreases in every cyclic process, the photocatalytic activity is retained over 90% of its original activity after five successive recycling experiments. The XRD patterns of $Zn_{0.97}Ni_{0.03}S$ sample before and after five consecutive photocatalytic reactions without obvious change are shown in Fig. 6(b). Meanwhile, the synthesized $Zn_{1-x}Ni_xS$ nanorods possess better photocatalytic activity for the degradation of RhB and are voluntarily reused in aqueous solution.

3.6 Photocatalytic mechanism

The possible mechanism of $Zn_{0.97}Ni_{0.03}S$ nanorods for the photodegradation of RhB is proposed in Fig. 7, which illustrates the redox reactions of photo-generated carriers under UV light irradiation. The band edge positions of the conduction band (CB) and valence band

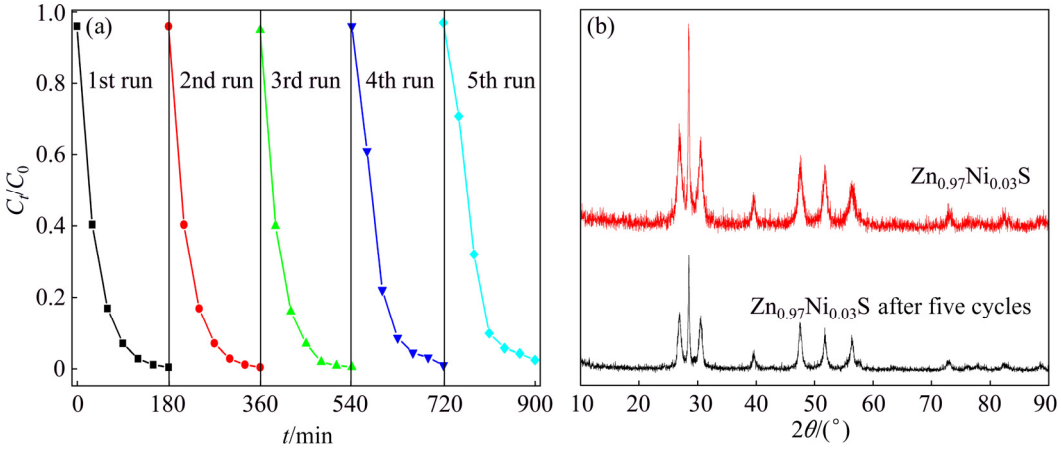

Fig. 6 Recyclability for photocatalytic degradation of RhB (a) and XRD patterns with and without five cycles (b) of $Zn_{0.97}Ni_{0.03}S$ nanorods

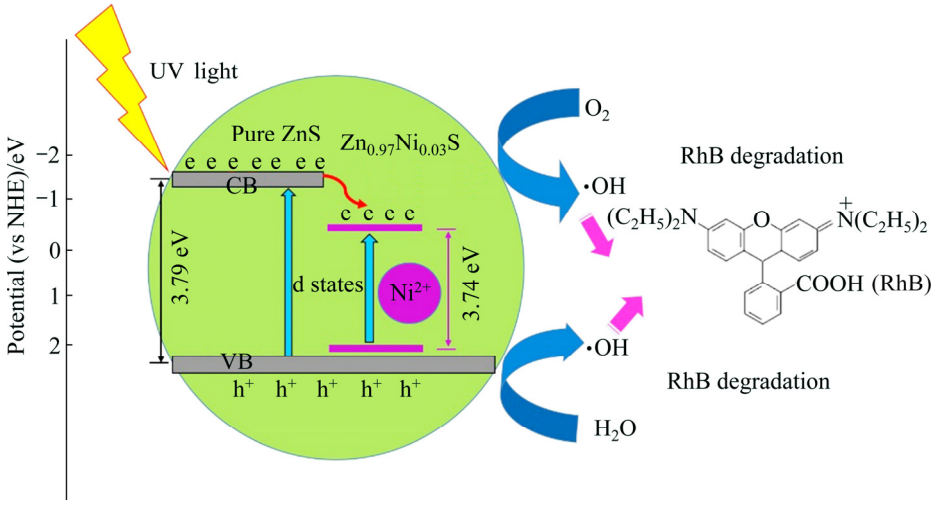

Fig. 7 Photocatalytic degradation mechanism of $Zn_{0.97}Ni_{0.03}S$ nanorods for photodegradation of RhB under UV light irradiation

(VB) of the ZnS nanoparticles can be determined using the following equations [16]:

$$E_{VB}=X-E_e+0.5E_g \quad (6)$$

$$E_{CB}=E_{VB}-E_g \quad (7)$$

where E_{VB} is the VB energy, E_{CB} is the CB energy, X is the electronegativity of the semiconductor, E_e is the free electron energy (4.5 eV, vs NHE), and E_g is the band gap. The CB and VB positions of ZnS and $Zn_{1-x}Ni_xS$ nanorods are qualitatively calculated:

$E_{CB}(ZnS)=-1.51$ eV, $E_{VB}(ZnS)=2.28$ eV;

$E_{CB}(Zn_{1-x}Ni_xS)=-1.46$ eV, $E_{VB}(Zn_{1-x}Ni_xS)=2.28$ eV.

The electrons (e) in the VB of ZnS are excited to the CB under UV light irradiation, leading to the generation of holes (h^+) in the VB of ZnS simultaneously. The doped ZnS effectively promotes the generation of photo-induced electron−hole pairs. The negative charge electrons in the VB jump to the CB by leaving positive charge holes on the VB (Eq. (8)). Because the doped ZnS reduces the average crystallite size and narrows the band gap, electrons from the CB move to the surface of the catalyst, which modifies the oxygen to superoxide anion radicals ($\cdot O_2^-$). The Ni^{2+} ions could facilitate the transfer of the photogenerated carriers by trapping the excited electrons. Conversely, the photo-generated holes on the VB are available to react with the water solution to form ·OH and H^+ (Eqs. (9) and (10)). Hydrogen ions (H^+) react with oxygen molecule to form hydrogen peroxide simultaneously (Eq. (11)). Furthermore, the generated hydrogen peroxide reacts with $\cdot O_2^-$ to form hydroxyl radicals (·OH), hydroxyl ions (OH^-) and oxygen molecule (O_2) (Eq. (12)).

These photo-generated hydroxyl radicals (·OH) acting as oxidant agents immensely react with the organic contaminates, which is favourable to the organic pollutant decomposition. Finally, ·OH and $\cdot O_2^-$ oxidize the RhB to CO_2, H_2O and other small molecule minerals (Eq. (13)) [17−19].

$$ZnS:Ni+h\nu \rightarrow ZnS:Ni(e)+ZnS:Ni(h^+) \quad (8)$$

$$ZnS:Ni(e)+O_2 \rightarrow ZnS:Ni+\cdot O_2^- \quad (9)$$

$$ZnS:Ni(h^+)+H_2O \rightarrow ZnS:Ni+\cdot OH+H^+ \quad (10)$$

$$O_2+H^+ \rightarrow H_2O_2 \quad (11)$$

$$H_2O_2+\cdot O_2^- \rightarrow \cdot OH+OH^-+O_2 \quad (12)$$

$$\cdot OH, \cdot O_2^- + \text{organic molecules} \rightarrow H_2O+CO_2+\text{minerals} \quad (13)$$

4 Conclusions

(1) $Zn_{1-x}Ni_xS$ nanorods with different Ni doping contents (x=0, 0.01, 0.03, 0.05 and 0.07) were synthesized by hydrothermal method. All $Zn_{1-x}Ni_xS$ nanorods synthesized using this method possess wurtzite structure with good crystallization. Ni^{2+} ions occupy the lattice site of Zn^{2+} to generate single-phase ZnS nanocrystals.

(2) The morphologies of all the samples are uniform one-dimensional nanorods with good dispersion. The crystalline size decreases and the shrink of lattice constant occurs as Ni^{2+} doping content increases. The band gap of $Zn_{1-x}Ni_xS$ nanocrystalline is smaller than that of pure ZnS, thus red shift occurs.

(3) The doped $Zn_{1-x}Ni_xS$ samples enhance photo-catalytic activities for the photodegradation of RhB under UV light irradiation. The $Zn_{0.97}Ni_{0.03}S$ sample exhibits the best photocatalytic performance and maximum rate constant.

References

[1] ASLAM S, MUSTAFA F, AHMAD M A, SALEEM M, IDREES M, BHATTI A S. Photovoltaic performance and impedance spectroscopy of ZnS−Cu−Go nanocomposites [J]. Ceramics International, 2018, 44: 402−408.

[2] WANG Jia-jia, TANG Lin, ZENG Guang-ming, ZHOU Yao-yu, DENG Yao-cheng, FAN Chang-zheng, GONG Ji-lai, LIU Ya-ni. Effect of bismuth tungstate with different hierarchical architectures on photocatalytic degradation of norfloxacin under visible light [J]. Transactions of Nonferrous Metals Society of China, 2017, 27: 1794−1803.

[3] ZHAO Wen-hua, WEI Zhi-qiang, WU Xiao-juan, ZHANG Xu-dong, ZHANG Li, WANG Xuan. Cr doped SnS_2 nanoflowers: preparation, characterization and photocatalytic decolorization [J]. Materials Science in Semiconductor Processing, 2018, 88(4): 173−180.

[4] ZHAO Xin-xin, YANG Hua, LI Shuai-hu, CUI Zi-ming, ZHANG Cai-rong. Synthesis and theoretical study of large-sized $Bi_4Ti_3O_{12}$ square nanosheets with high photocatalytic activity [J]. Materials Research Bulletin, 2018, 107: 180–188.

[5] HOROZ S. Effect of Eu^{2+} doping on structural, optical, magnetic and photovoltaic properties of ZnS quantum dots [J]. Superlattices and Microstructures, 2017, 111: 1043−1049.

[6] LIU Kui-li, LI Ji-tao, LIU Quan-tao, MENG Ming, HU Ling-wei, XU Chun-xiang. Two-photon absorption induced photoluminescence from ZnS nanowires [J]. Journal of Alloys and Compounds, 2017, 718: 122−125.

[7] VIRPAL, KUMAR J, THANGARAJ R, SHARMA S, SINGH R C. Enhanced dielectric permittivity and photoluminescence in Cr doped ZnS nanoparticles [J]. Applied Surface Science, 2017, 416: 296−301.

[8] CAI Dong, YUAN Xi, ZHU De-hua, ZHOU Hong-ming, LI Hai-bo, ZHAO Jia-long. Al-doped ZnS shell as a surface shield for enhancing the stability of Cu: ZnInS/ZnS/ZnS: Al quantum dots and their application in light emitting diodes [J]. Materials Research Bulletin, 2017, 94: 241−246.

[9] SAHRAEI R, MOHAMMADI F, SOHEYLI E, ROUSHANI M. Synthesis and photoluminescence properties of Ru-doped ZnS quantum dots [J]. Journal of Luminescence, 2017, 187: 421−427.

[10] CHEN S Q, ZAEIMIAN M S, MONTEIRO J, ZHAO J L, MAMALIS A G, DE BETTENCOURT-DIAS A, ZHU X S. Mn doped AIZS/ZnS nanocrystals: Synthesis and optical properties [J]. Journal of Alloys and Compounds, 2017, 725: 1077−1083.

[11] TRUNG D Q, THANG P T, HUNG N D, HUY P T. Structural evolution and optical properties of oxidized ZnS microrods [J]. Journal of Alloys and Compounds, 2016, 676: 150−155.

[12] JOTHIBAS M, MANOHARAN C, JOHNSON JEYAKUMAR S, PRAVEEN P, KARTHARINAL PUNITHAVATHY I, PRINCE RICHARD J. Synthesis and enhanced photocatalytic property of Ni doped ZnS nanoparticles [J]. Solar Energy, 2018, 159: 434−443.

[13] BAI Jin-wu, LI Yun, JIN Peng, WANG Jun-feng, LIU Lu. Facile preparation 3D ZnS nanospheres-reduced graphene oxide composites for enhanced photodegradation of norfloxacin [J]. Journal of Alloys and Compounds, 2017, 729: 809−815.

[14] ZHAO Wen-hua, WEI Zhi-qiang, ZHU Xue-liang, ZHANG Xu-dong, JIANG Jin-long. Optical and magnetic properties of diluted magnetic semiconductors $Zn_{0.95}M_{0.05}S$ nanorods prepared by hydrothermal method [J]. International Journal of Materials Research, 2018, 109(5): 405−412.

[15] ASHOK KUMAR M, MUTHUKUMARAN S. Effect of deposition time on structural, optical and photoluminescence properties of $Cd_{0.9}Zn_{0.1}S$ thin films by chemical bath deposition method [J]. Journal of Materials Science: Materials in Electronics, 2013, 24: 2858−2865.

[16] SUBRAMANYAM K, SREELEKHA N, AMARANATHA REDDY D, MURALI G, RAHUL VARMA K, VIJAYALAKSHMI R P. Chemical synthesis, structural, optical, magnetic characteristics and enhanced visible light active photocatalysis of Ni doped CuS nanoparticles [J]. Solid State Sciences, 2017, 65: 68−78.

[17] SREELEKHA N, SUBRAMANYAM K, AMARANATHA REDDY D, MURALI G, RAHUL VARMA K, VIJAYALAKSHMI R P. Efficient photocatalytic degradation of rhodamine-B by Fe doped CuS diluted magnetic semiconductor nanoparticles under the simulated sunlight irradiation [J]. Solid State Sciences, 2016, 62: 71−81.

[18] REDDY D A, CHOI J, LEE S, KIM Y, HONG S, KUMAR D P, KIM T K. Hierarchical dandelion-flower-like cobalt−phosphide modified CdS/reduced graphene oxide−MoS_2 nanocomposites as a noble-metal-free catalyst for efficient hydrogen evolution from water [J]. Catalysis Science & Technology, 2016, 6: 6197−6206.

[19] ISLAM M J, REDDY D A, CHOI J, KIM T K. Surface oxygen vacancy assisted electron transfer and shuttling for enhanced photocatalytic activity of a Z-scheme CeO_2−AgI nanocomposite [J]. RSC Advances, 2016, 6: 1934−19350.

水热法制备镍掺杂 ZnS 纳米棒的显微组织与光催化性能

赵文华[1,2]，魏智强[1,2]，武晓娟[1]，张旭东[2]，张 莉[2]，王 璇[2]

1. 兰州理工大学 省部共建有色金属先进加工与再利用国家重点实验室，兰州 730050；
2. 兰州理工大学 理学院，兰州 730050

摘 要：采用水热法合成纯 ZnS 和 Ni 掺杂 ZnS 纳米棒。通过 X 射线衍射(XRD)、高分辨透射电子显微镜(HRTEM)、色散能量分析谱仪(EDS)和紫外可见吸收光谱(UV−Vis)等技术分别研究 Ni 掺杂对样品的物相结构、形貌、元素组成和光学性能的影响，并通过紫外光照射在水溶液中降解有机染料罗丹明 B(RhB)研究 $Zn_{1-x}Ni_xS$ 纳米棒的光催化活性。结果表明：所有样品具有纤锌矿结构，结晶良好。样品的形貌均为一维纳米棒结构，分散性较好，晶格常数发生畸变。掺杂 $Zn_{1-x}Ni_xS$ 的带隙小于纯 ZnS 的，因此，发生红移现象。Ni 掺杂 ZnS 纳米材料能增强降解有机染料罗丹明 B 的光催化活性，尤其是 $Zn_{0.97}Ni_{0.03}S$ 样品对罗丹明 B 具有较好的光催化性能和光催化稳定性。

关键词：$Zn_{1-x}Ni_xS$ 纳米棒；物相结构；显微组织；光催化活性；水热法

(Edited by Wei-ping CHEN)